Clinical Biomechanics 131 (2026) 106723

Contents lists available at ScienceDirect

Clinical Biomechanics

journal homepage: www.elsevier.com/locate/clinbiomech

Fluted stem designs enhance surgical precision and primary stability in cementless revision hip arthroplasty – A cadaver study

Julius M. Boettcher [a,*], Kay Sellenschloh [a], Ana Cruz Pardos [b], Gerd Huber [a], Benjamin Ondruschka [c], Michael M. Morlock [a]

[a] Institute of Biomechanics, TUHH Hamburg University of Technology, Hamburg, Germany
[b] Department of Traumatology and Orthopaedic Surgery, Hospital Universitario La Paz, Madrid, Spain
[c] Institute of Legal Medicine, University Medical Center Hamburg-Eppendorf, Hamburg, Germany

ARTICLE INFO

Keywords:
Cementless revision hip arthroplasty
Hip revision stem
Primary stability
Implant design
In-vitro experiment
Biomechanical cadaver study

ABSTRACT

Background: Cortical contact of the stem is a key determinant for primary stability in cementless revision hip arthroplasty. This matched-pair cadaveric study evaluated whether implant designs that increase cortical contact improve primary fixation of cementless revision stems

Methods: Ten paired femora received either a tapered monoblock RECLAIM™ stem with advanced spline (RAS) geometry or an identically sized prototype solid stem. Axial seating and rotation were recorded using dynamic image correlation during implantation. Specimens were cyclically loaded up to 200 % body weight, after which torque-to-failure was measured

Findings: Both designs showed mean micromotion <50 μm during cyclic loading, consistently favourable for osseointegration. However, solid stems rotated more during implantation than RAS stems ($3.6 \pm 5.0^\circ$ vs. $0.5 \pm 0.6^\circ$, $p = 0.088$). The cortical contact area of the solid stems was 43.6 % larger than RAS stems ($p < 0.001$) without an impact on superior fixation: Axial subsidence and rotation during cyclic loading did not differ significantly between the designs but two solid-stem specimens fractured under high loading. Torque-to-failure of the RAS stems was 38.7 ± 7.5 nm, exceeding that of solid stems by 24.3 % ($p = 0.032$)

Interpretation: These findings suggest that maximising circumferential contact by implant design alone cannot compensate for irregularities of the femoral canal. Whereas solid stems wedge firmly only at the cost of positioning accuracy and increased fracture risk, the thin splines of the RAS design engage the cortex progressively, guide the implant to the planned depth, and augment torsional resistance without excessive press-fit. Tapered stems with cortex-indenting splines improve primary stability in cementless revision hip arthroplasty more effectively than increasing contact area alone.

1. Introduction

The number of total hip arthroplasties continues to increase worldwide with a high absolute number of revision procedures (rTHA) despite a relative decrease in revision incidence (Jones et al., 2025). Current national registries such as the German Endoprosthesis Registry (EPRD (Grimberg et al., 2024)), the National Joint Registry of UK, Ireland and the Isle of Man (NJR (NJR, 2024)) or the American Joint Replacement Registry (AJRR (AAOS, 2024)) continue to document high revision numbers, especially in ageing patient cohorts. With increasing age, reduced bone quality and bone defects due to osteolysis and multiple surgeries as well as re-revisions with complex femoral reconstructions are occurring more frequently (Sheth et al., 2013).

Periprosthetic joint infection remain a major concern for re-revision (AAOS, 2024; Grimberg et al., 2024; NJR, 2024) but also the principal mechanically mediated indications for femoral revision as aseptic loosening, femoral component instability or recurrent dislocation, and periprosthetic femoral fracture are of concern. The mechanical reasons for revision are frequently interrelated and can often be traced to inadequate direct-postoperative implant fixation. Registry surveillance and institutional series consistently place these mechanical reasons among the leading reasons for rTHA, with relative contributions that vary by registry and year but that collectively exceed those of the non-mechanical indications (Jones et al., 2025; Kelmer et al., 2021).

* Corresponding author.
E-mail address: julius.boettcher@tuhh.de (J.M. Boettcher).

https://doi.org/10.1016/j.clinbiomech.2025.106723
Received 17 September 2025; Accepted 26 November 2025
Available online 27 November 2025

Mechanical failure pathways result in the loss of construct stability at the bone–implant interface. Successful osseointegration of porous or roughened metal surfaces occurs only if the relative micromotion remains below 50 μm; larger motions foster fibrous tissue interposition and subsequent loosening (Jasty et al., 1997; Kohli et al., 2021). Radiographic analyses of cementless stems have linked early subsidence to an increased long term risk of aseptic femoral loosening, reinforcing the importance of secure direct-postoperative fixation for survivorship (Streit et al., 2016).

Stem design plays an important role for early stability, especially when proximal femoral bone stock is compromised (Amanatullah et al., 2015; Della Valle and Paprosky, 2003). Early cylindrical or extensively coated stems allowed to achieve diaphyseal fixation, but were associated with stress shielding, subsidence in femurs with deficient metaphyses, and technically difficult surgeries in severely damaged femora (Engh et al., 1987; Engh et al., 1988; Lawrence et al., 1994). Progressive adoption of conical, self-locking revision stems - exemplified by the Wagner family of designs (Wagner, 1987, 1989) - demonstrated that a tapered geometry can generate axial stability by wedging within the diaphysis, facilitating reconstruction even across substantial bone defects. Mid to long term series report reliable fixation and good longterm results using this concept with less associated stress shielding, radiolucency and thigh pain compared to cylindrical fully coated stems. (Böhm and Bischel, 2004; Hartwig et al., 1996; Hernández-Mateo et al., 2024; Regis et al., 2011).

Modern tapered revision stems commonly incorporate longitudinal splines intended to enhance rotational stability by indenting the endosteal cortex while preserving the axial wedging effect of the taper geometry. Parametric testing has shown that taper angle and spline geometry influence initial mechanical stability under axial loading (Pierson et al., 2015). Matched pair cadaveric studies varying stem–cortex engagement length reported that greater diaphyseal contact improves resistance to subsidence, and supplementary investigations suggest similar benefits when cortical engagement is augmented in deficient proximal bone (Boettcher et al., 2025; Gkiatas et al., 2021; Kendrick et al., 1995). Rotational stability under torsional load appears particularly sensitive to spline configuration when proximal support is reduced and improves with a second set of less prominent, wider splines that increase cortical contact (Boettcher et al., 2023).

The purpose of the present study was to investigate the influence of increasing the amount of diaphyseal cortical contact on direct-postoperative mechanical stability. A prototype solid, tapered, cementless monoblock stem was designed and manufactured – theoretically maximising circumferential diaphyseal engagement - and compared to a cortex indenting RECLAIM™ Advanced Spline (RAS) stem design in terms of implantation accuracy and direct-postoperative stability in a matched pair cadaveric study.

2. Methods

Ten matched pairs of fresh-frozen human femora (73.8 ± 8.7 years, 8 male, 2 female donors, body mass index: 29.4 ± 4.6 kg/m^2) were sourced by the Institute of Legal Medicine Hamburg. All patient-level data were anonymized, and the protocol was sanctioned by the Ethics Committee of the Hamburg Medical Association (2023–300,350-WF).

CT scans (Incisive CT 128; Philips, Amsterdam, The Netherlands; isotropic voxel size: 0.4 mm^3) of the bones prior to the experiments were acquired with a calibration phantom included in every slice (QSA; QRM, Moehrendorf, Germany). Measured Hounsfield units were then converted to bone mineral density (BMD) in terms of hydroxyapatite content (Structural Insight 3; University Medical Center Schleswig-Holstein (Graeff et al., 2007), Kiel, Germany). Mean cortical BMD was determined in a 10 mm circumferential band of the femoral shaft positioned 5.8 % of the donor's body height below the lesser trochanter (threshold: 400–2000 mgHA/ml (Bätz et al., 2019; Boettcher et al., 2025), Matlab R2024b; The Mathworks, Natick, MA). Bone morphology was quantified using a donor-specific Dorr classification and the canal-to-calcar ratio (CCR), while trabecular BMD was derived from a 1000 mm^3 spherical region of interest (ROI) at the femoral head's center (Boettcher et al., 2025).

2.1. In-vitro experiment

Cementless hip revision stems with the RECLAIM™ Advanced Spline (RAS) design (Stem length: 185 mm; RECLAIM™ Monobloc Hip System; DePuy Orthopaedics, Warsaw, IN) were implanted into one femur of each pair after standard femoral canal preparation. On the contralateral side, 3D-printed, grit-blasted solid stems without splines were implanted. The diameter of the solid stems was determined using the diameter of the secondary splines of the RAS design of the respective size (Fig. 1). To minimize the risk of femoral fracture, press-fit was reduced from 0.5 mm for the RAS stems to 0.1 mm for the solid stems by means of deeper reaming. This decision was based on preliminary experiments in which using a 0.5 mm press-fit for the solid stems resulted in an unacceptably high rate of fractures during implantation, preventing completion of the test protocol.

Powered reaming was performed by an experienced orthopaedic surgeon using helical reamers of the RECLAIM™ system according to the manufacturer's instructions. Implant size planning was performed with CT-derived radiographs (VELYS™ Hip Navigation v4.5.0.54, DePuy Orthopaedics, Warsaw, IN). The colored marks on the instruments were used to determine the final reaming position in relation to the greater trochanter intraoperatively. To account for the reduced press-fit of the solid stems, an additional mark was placed on the reamer extension, located 4.6 mm proximal which corresponds to a 0.4 mm decrease in diameter for a taper angle of 2.5° (Fig. 2). After reaming, the specimens were embedded in a bone cement equivalent two-component polymer (Technovit 4004; Kulzer GmbH, Wehrheim, Germany) with two screws placed through the distal cortex to prevent relative motion and a second femoral CT scan was obtained. Bone samples were wrapped in paper towels soaked with Ringer's solution, double-bagged in sealed plastic bags to prevent freeze-drying, and refrozen until testing.

At the day of the experiments, the bones were fully thawed at room temperature while still wrapped in paper towels soaked with Ringer's solution. Dynamic implantation was then performed with a drop tower to receive consistent implantation instead of those by variable mallet blows (Fig. 3A). Impact energy started at 2 J (5 kg drop weight, 40 mm

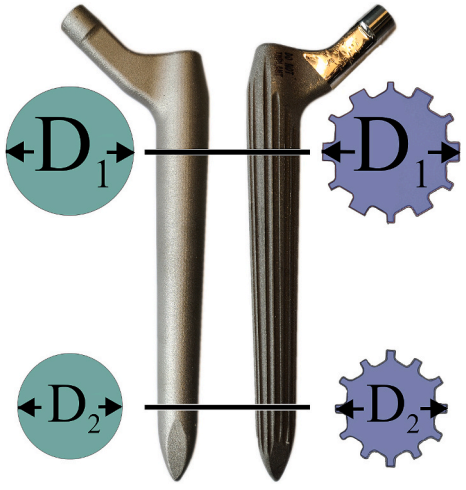

Fig. 1. The solid stems for this study were designed to match the diameter of the secondary, wider splines of the RAS stem in the RECLAIM™ system (D1: The wide splines are approximately 2x wider than the thin splines, D2: All splines of the RAS design are of equal width). These splines are 0.25 mm less prominent than the thin splines equalizing to the thin splines distally. Implant length, offset, and distal taper geometry are identical for the two designs.

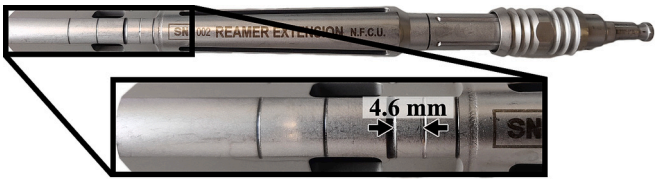

Fig. 2. Using the same RECLAIM™ system reamer extension, an experienced orthopaedic surgeon prepared the cavities for both stem designs. The etched reference line indicated the final reaming depth once aligned with the greater trochanter. To obtain the reduced 0.1 mm press-fit for the solid stems (instead of the standard 0.5 mm), an additional mark was placed 4.6 mm proximally (indicated in the figure).

drop height) and was successively increased by 1 J increments to a maximum of 5 J unless incremental stem seating per hit was <0.5 mm. The 5 J ceiling corresponds to a representative surgical-mallet blow in order to avoid excessive fractures (Maharaj and Jamison, 1993). Both the number of hammer blows required to reach the implant position that was determined by the reaming as all as the impact energy of each blow were recorded. Axial impaction forces were measured between the implant adapter and the impactor using a uniaxial force cell (50 ms, 800 kHz, 9333a; Kistler Instrumente, Winterthur, Switzerland). Dynamic stem seating and rotation were captured with a digital image correlation system (DIC, Measuring accuracy 0.01 pixel, optimized calibration error analogous to (Schroeder et al., 2022), 25 fps, FOV: 2752 × 2200 px, marker size: 0.4 mm; ARAMIS 3D Camera; Carl Zeiss, Braunschweig, Germany, (Boettcher et al., 2025)).

After implantation, ceramic ball heads (28 mm, 12/14 L) were assembled to the stem tapers. The specimens were mounted in a servo-hydraulic testing machine and subjected to cyclic loading via the ball head (1 Hz) at two load levels, each applied for 600 cycles (force-controlled, load level low: peak-to-peak 80–800 N, load level high: peak-to-peak 80–1600 N; MiniBionix II; MTS, Eden Prairie, MN; (Fig. 3B)). The lower valley load of 80 N was chosen to avoid complete unloading and to maintain continuous contact at the head–liner interface, while the peak loads of 800 N and 1600 N correspond approximately to 100 % and 200 % body weight for an 80 kg patient, thereby representing full weight-bearing during standing and level walking. The total of 600 cycles per level was selected to provide a reproducible comparative loading protocol between stem designs and to approximate repeated early postoperative loading over several hundred gait cycles, rather than to simulate long-term fatigue behavior, which cannot be simulated well in an in-vitro setting with human specimens. The proximal load application was unrestricted in the horizontal direction while the distal end was restricted in all degree of freedom. The specimen were aligned according to ISO 7206-4 (ISO/TC 150 Implants for Surgery, 2020) (10° lateral and 9° dorsal tilt of the implant axis relative to the loading axis). The position was adjusted using a magnetic 2D spirit level on top of an angled implant adapter in combination with a distal ball-and-socket clamp as an adjustable fixture. Relative bone-stem motion was recorded with a DIC system for the first and last 10 s of each cyclic loading and in five equally spaced segments in between. Axial translation of the implant along its stem axis and its rotation about this axis were quantified (Boettcher et al., 2023, 2025). Subsidence was defined as the change in mean axial displacement between the first and last measurement segments of the test. Micromotion was defined as the change in the standard deviation of axial displacement for the same region and interval; the standard deviation was chosen for its statistical robustness, as for an ideal harmonic oscillation it is approximately 70 % of the amplitude. Rotational relative motion was assessed analogously.

Following cyclic loading, the specimens were aligned with the machine axis with an X-Y table and tested in torque to failure using a separate servo-hydraulic machine (0.5°/s, angle-controlled; 100 N axial preload, force-controlled; MiniBionix II, MTS, Eden Prairie, MN; (Fig. 3C)). Failure was defined as a sudden drop in the moment–time curve, indicating slip at the bone-implant interface. Each specimen was hereby mounted coaxially with the machine axis to prevent bending moments, and torque was applied via a stem adapter. (Boettcher et al., 2023). Throughout testing, the bones were kept moist with Ringer's solution.

2.2. Contact analysis

Contact pattern between stems and cortical bones were generated to identify differences between the stem designs regarding cortical contact and to evaluate the uniformity of contact for the solid stems. Surface models of the cortices were segmented from the CT images (threshold: [400–2000 mgHA/ml], Avizo Lite 2020.2; Thermo Fisher Scientific, Waltham, MA) and superimposed by surface models derived from high-resolution 3D laser scans (scan resolution of 0.012 mm; HandySCAN Black+™|Elite; Creaform, Quebec, Canada) of the implants and of the implanted stems together with the bone after implantation. The laser scan of the implant-bone-construct enabled alignment of the implant model with the model of the cortical bone, so that the relative position of the implant with respect of the achieved cavity after reaming was available (PolyWorks Metrology Suite 2020; InnovMetric Software Inc., Quebec, Canada; (Fig. 4A)). A semi-automatic iterative closest point

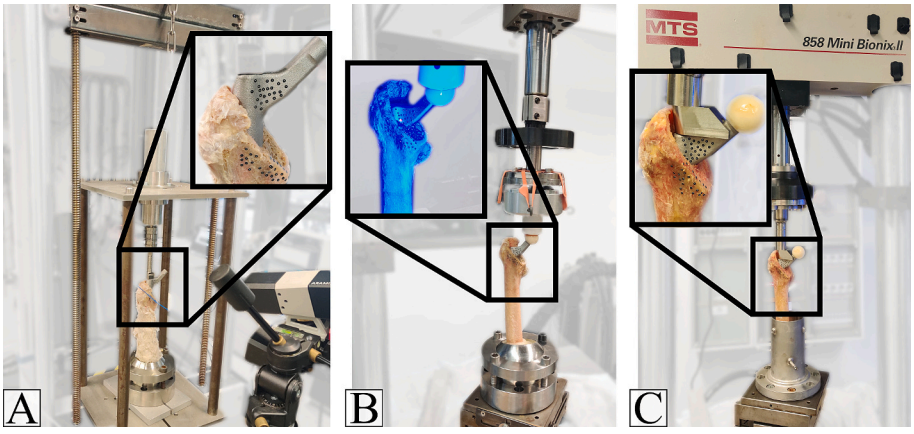

Fig. 3. Images of the combined workflow: (**A**) A drop tower was employed for axial implantation to eliminate variability from manual mallet blows. Digital image correlation with optical markers on bone and stem were used to quantify relative motion along and around the implant axis. (**B**) A ball-and-socket fixture was used to align the bones according to the ISO specifications for cyclic loading; the DIC markers were used to determine micromotion and stem subsidence. (**C**) After cyclic loading, each specimen was mounted coaxially in a second test machine for torque-to-failure testing, with an X-Y table ensuring precise alignment of the specimen to the machine axis.

(ICP) algorithm was applied manually selecting prominent landmarks such as the greater and lesser trochanter (Fig. 4B). As optimization criterion for the ICP algorithm the residual root mean square error (RMSE) was set below 0.012 mm which corresponds to the resolution of the 3D laser scanner (Fig. 4C). The native bone model prior to reaming was aligned identically.

The indentation depth of the splines of the RAS design as well as general overclosure of the stems with the cortical cavity was evaluated as the overlap of the implant models and the respective reamed bone models in the x- and y-directions, while the z-axis was defined to coincide with the implant axis. Between the implant neck and the stem tip, each slice of 1 mm height was divided into 120 sectors of 3° opening angle each, starting at 0° medially. In these sectors the location and the size of the overlap between the implant and the cortical bone (Fig. 5A) were determined and illustrated as contact maps which show coherent contact areas (Fig. 5B).

Models were evaluated from the lesser trochanter to 190 mm distal to the greater trochanter, corresponding to the final position of the RECLAIM™ reamer tip per the surgical technique (Fig. 6A). To quantify the influence of bone preparation on contact uniformity and the resulting primary stability under load, cortical bone cavities were not only investigated for reamed bones but also for the native bone to determine the removed cortical bone during reaming. The effectiveness of creating a conical cavity was further assessed by analyzing the roundness of 19 equally spaced cross-sectional contours. Roundness was quantified as

$$r = \frac{1 - (r_{max} - r_{min})}{r_{max}}$$

where r_{max} and r_{min} are the maximum and minimum distances from the centroid of the respective cross-section to the boundary points. For r equal 1 a perfectly circular cross-section is achieved, whereas values closer to 0 indicate a more elongated or irregular shape (Fig. 6B).

2.3. Statistical analysis

Statistical analyses were conducted at $\alpha = 0.05$ as significance level (IBM SPSS Statistics 26; IBM, Armonk, NY). Normality and homoscedasticity were assessed with the Shapiro-Wilk and Levene tests. Within-pair differences were evaluated using paired *t*-tests. Associations among variables were examined with Pearson correlations.

3. Results

Neither cortical BMD (1142 ± 53 mgHA/ml) nor trabecular BMD (369 ± 60 mgHA/ml) differed significantly between femoral pairs ($p_{cortical} = 0.225$; $p_{trabecular} = 0.163$; paired *t*-tests) or between the two stem design test groups ($p_{cortical} = 0.858$; $p_{trabecular} = 0.557$; unpaired t-tests). Bone morphology within femoral pairs was similar regarding Dorr type ($p > 0.99$; paired *t*-test), cortical index ($p = 0.834$; paired t-test), and the CCR of the femoral canal ($p = 0.976$; paired t-test).

3.1. Cavity preparation

The cortical bone volume removed during reaming did not differ statistically between groups, despite over-reaming to achieve reduced press-fit in the solid-stem design (RAS: 1.47 ± 0.52 cm^3; solid: 1.54 ± 0.58 cm^3; $p = 0.812$; paired t-test). Cavity roundness improved with reaming from 0.58 ± 0.06 (initial femoral canal) to 0.63 ± 0.07 but remained well below the theoretical optimum of 1.0. Across the 19 analyzed cross-sections, the maximum roundness increase was 0.10 at 35 % and 80 % evaluation heights. There was no difference between the groups in cavity roundness either before or after reaming ($p_{before} = 0.383$, $p_{after} = 0.499$; paired *t*-test). The angular difference between the principal axes of the initial and reamed cavities was also not statistically significant and generally low (RAS: 0.35 ± 0.26°; solid: 0.49 ± 0.37°; $p = 0.301$; paired *t*-test). The mean difference in cavity roundness showed a significant negative correlation with Dorr type, indicating less effective reaming with increasing proximal canal morphology ($R^2 = 0.286$; $p = 0.015$; Pearson correlation), and a positive correlation with cortical index ($R^2 = 0.221$; $p = 0.036$; Pearson correlation).

3.2. Implantation

The cumulative implantation force was 30 % higher for the RAS stem but not statistically significant (RAS: 36.5 ± 12.3 kN; solid: 28.0 ± 10.9 kN; $p = 0.123$; paired *t*-test; (Fig. 7A)). Similarly, the number of drop tower hits did not differ significantly; the RAS design per trend required one additional hit on average (RAS: 9.8 ± 2.4 hits; solid: 8.8 ± 2.0 hits; $p = 0.293$; paired *t*-test). No significant correlations were found between implantation force and either BMD or bone-morphology metrics. No fractures occurred during stem insertion anywhere. Relative to the target implantation depth of 185 mm (implant tip to greater trochanter) specified by the surgical technique, deviation was significantly smaller for the RAS stem (RAS: −1.35 ± 3.96 mm; solid: −5.30 ± 2.48 mm; $p = 0.049$; paired *t*-test; (Fig. 7B)). The subsidence during implantation was significantly lower for the RAS stem for each of the first three consecutive strikes performed at 2 J (Table 1) as was the overall stem subsidence during implantation (RAS: 10.9 ± 4.2 mm; solid: 16.9 ± 5.5 mm; $p = 0.025$; paired *t*-test; Fig. 7C).

Stem rotation during implantation was lower with the RAS design but not statistically significant (RAS: 0.54 ± 0.56°; solid: 3.61 ± 4.97°; $p = 0.262$; paired *t*-test; (Fig. 7D)).

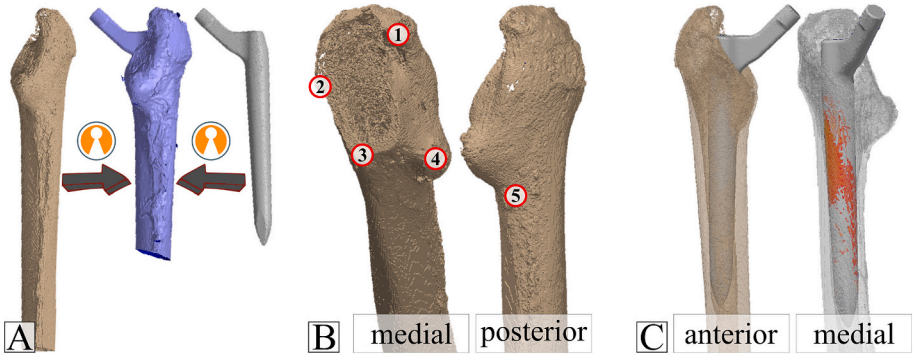

Fig. 4. Alignment workflow for the surface models used in the contact analysis. (A) A 3D laser scan of the femur with the implanted stem served as reference; the segmented reamed cortex and corresponding stem scan were aligned using a semi-automatic ICP algorithm in PolyWorks Inspector. (B) Five prominent landmarks were manually selected to initialise the automatic alignment. (C) The final registration enabled high-resolution overclosure analysis between the reamed cavity and the stem and visualisation of coherent contact areas.

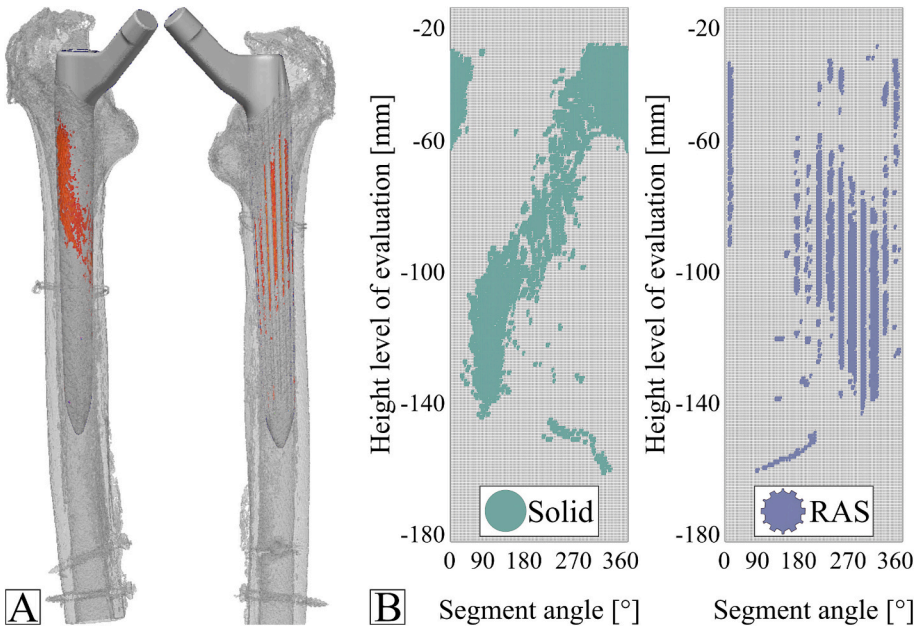

Fig. 5. Quantification of the implant–bone interface for the solid and RAS stem designs. (A) Overclosure between implant and cortex is shown for the solid stem (left) and the RAS stem (right), illustrating contact location and uniformity. (B) The resulting contact maps were used to determine contact length, anatomical position relative to the body axes, and circumferential coverage; the spatial resolution allows clear distinction between the thin and the wider, less prominent splines of the RAS design.

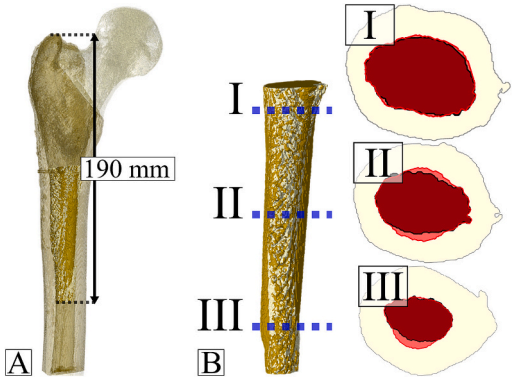

Fig. 6. Cavity geometry before and after reaming. (A) Cortical cavities of the native and reamed femora were segmented and aligned to each bone; the region of interest extended from the lesser trochanter to a plane 190 mm distal to the greater trochanter, corresponding to the distal end position of the reamer tip. (B) Representative cross-sections comparing the initial (deep red with black border) and reamed (bright red with red border) cavities at three equidistant levels.

3.3. Contact analysis

The solid stem design achieved 43.6 % greater cortical contact than the RAS design (RAS: 68.9 ± 12.3 mm^2; solid: 122.1 ± 11.3 mm^2; $p < 0.001$; paired t-test; (Fig. 8A)). Similarly, the average segmental contact length on the observed contact maps differed significantly between designs (RAS: 15.0 ± 4.9 mm; solid: 31.1 ± 6.1 mm; $p < 0.001$; paired t-test). Contact area and contact length were strongly correlated ($R^2 = 0.67$; $p < 0.001$; Pearson correlation). Average implant indentation at the bone–implant interface was significantly greater for the RAS design, reflecting the increased press-fit (RAS: 0.246 ± 0.035 mm; solid: 0.150 ± 0.026 mm; $p < 0.001$; paired *t*-test; (Fig. 8B)). Neither contact area nor overclosure correlated with BMD or bone morphology metrics.

3.4. Cyclic loading

No statistically significant differences were found in micromotion, angular micromotion, rotation, or subsidence between the two stem designs at either load level. The change in micromotion from the first measurement section at the first load level (80–800 N) to the last measurement section at the higher load level (80–1600 N) after 600 loading cycles was equally low for both designs (RAS: 21.8 ± 26.21 μm; solid: 18.7 ± 23.9 μm; $p = 0.859$; paired t-test; (Fig. 8C)). After 600 loading cycles, stem subsidence was approximately sevenfold higher with the solid design, but the difference was not statistically significant given the large variability of the solid design (RAS: 0.04 ± 0.03 mm; solid: 0.32 ± 0.57 mm; $p = 0.153$; paired t-test). Similarly, rotation induced by cyclic loading was lower for the RAS design (RAS: 0.01 ± 0.38°; solid: 0.51 ± 1.42°; $p = 0.300$; paired t-test). Two femora implanted with the solid stem design fractured during cyclic loading at the first measurement section of the higher load level. The two specimens that failed during cyclic loading were excluded from further analysis. No significant correlation was found between any of the four relative motions analyzed and bone morphology metrics or BMD, except for stem micromotion, which correlated negatively with Dorr type, representing proximal femur morphology ($R^2 = 0.235$; $p = 0.041$; Pearson correlation).

3.5. Torque to failure

Torque-to-failure testing of the remaining femoral pairs ($n = 8$) showed significantly greater resistance to torsional loading for the RAS stem compared with solid stems by 24.3 % (RAS: 38.7 ± 7.5 Nm; solid: 29.3 ± 10.7 Nm; $p = 0.032$; paired t-test; (Fig. 8D)). The elastic stem-femur relative angle until slip (corresponding to interface failure) was also larger with the RAS design (RAS: 6.6 ± 1.6°; solid: 4.0 ± 1.7°; $p = 0.030$; paired t-test). Torque to failure did not correlate with bone morphology-related measures or with cortical or trabecular BMD. However, stem subsidence during cyclic loading correlated negatively with torque to failure ($R^2 = 0.36$; $p = 0.008$; Pearson correlation), indicating that interface instability reduces resistance to torsional loading.

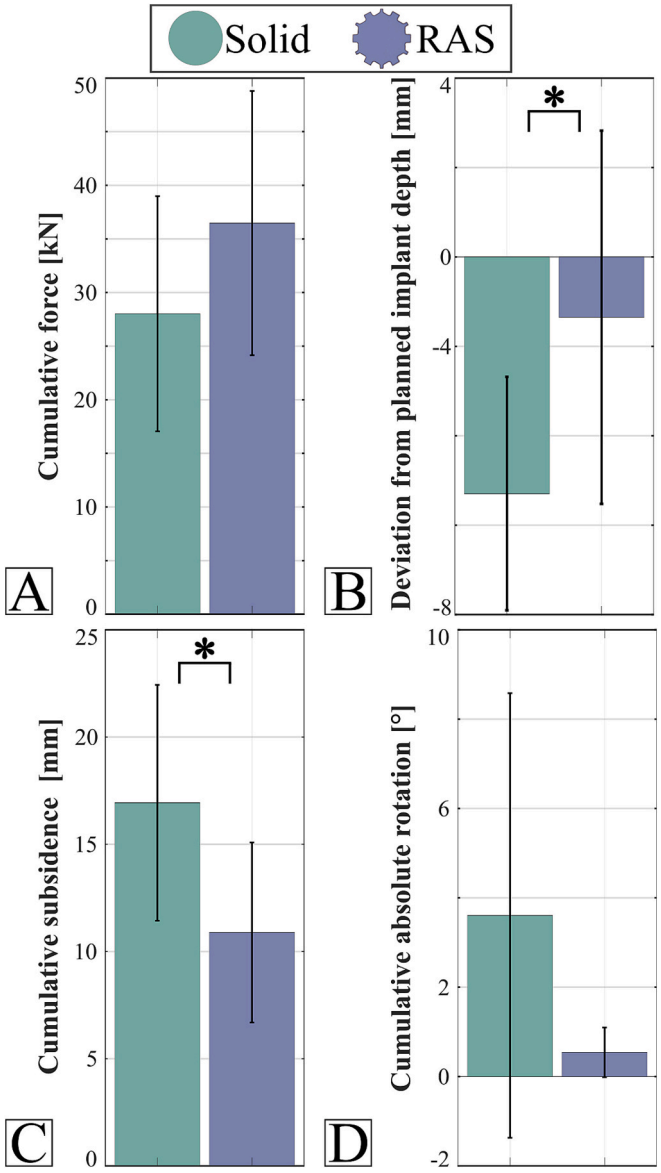

Fig. 7. Comparison of the stem implantation process for the two designs. (**A**) The cumulative implantation force was higher for the RAS design, but the difference was not statistically significant ($p = 0.123$). (**B**) The deviation from the planned implant depth (by means of ideal reaming) was significantly increased for the solid stem, indicating less precise axial positioning with all stems being implanted too deep ($p = 0.049$). (**C**) Similarly, the cumulative subsidence during implantation was significantly greater for the solid stem ($p = 0.025$). (**D**) Undesired stem rotation was also higher for the solid stem compared with the RAS stem, though this was not statistically significant ($p = 0.262$).

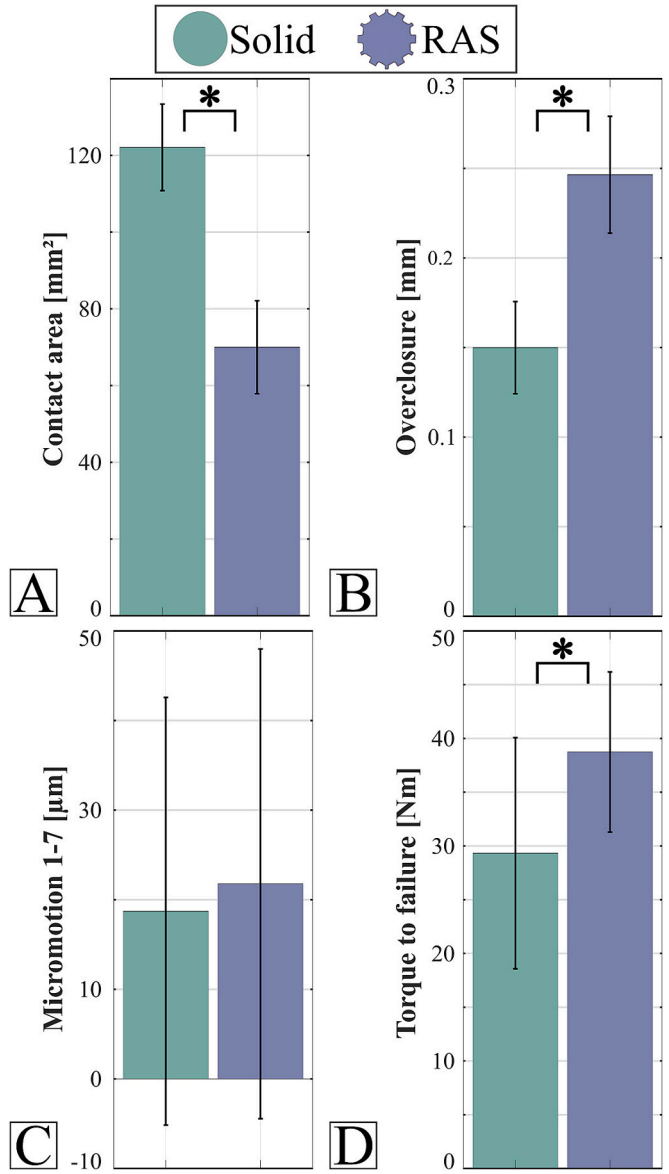

Fig. 8. Comparison of contact and primary stability parameters between the solid and the RAS stem design demonstrated: (**A**) the solid stem had a significantly larger contact area ($p < 0.001$); (**B**) the RAS experienced greater indentation into the cortical bone, indicating the stronger press-fit ($p < 0.001$); (**C**) micromotion under cyclic loading did not differ significantly ($p = 0.815$); and (**D**) torque to failure was significantly higher for the RAS design ($p = 0.032$).

Table 1
Comparison of stem subsidence between the two designs during implantation for the first three 2 J drop tower hits.

Hit no.	RAS Mean ± SD [mm]	Solid Mean ± SD [mm]	*p*-value (paired *t*-test)
1	5.18 ± 2.30	7.68 ± 2.48	0.016
2	1.46 ± 0.81	2.85 ± 1.00	0.008
3	0.82 ± 0.55	1.83 ± 0.81	0.019

4. Discussion

The RAS spline design, which incorporates a second set of less prominent, wider splines, was shown to outperform the standard design without the second set of splines with respect to rotational and axial stability in two own prior in vitro studies (Boettcher et al., 2023, 2025). The present study investigated the effect of maximized cortical contact at the bone-implant interface, which had been identified as a decisive factor for immediate postoperative stability, by comparing solid prototypes without splines with the RAS stem design. The hypothesis was that increasing cortical contact area enhances primary stability only when combined with splines, since femoral morphology precludes circumferential contact over a sufficient length without the removal of excessive amounts of bone. The results were unambiguous: although cortical contact was significantly greater for the solid stem design, the

strength of the bone-implant interface was lower than with the RAS design, particularly during implantation and torque-to-failure testing. These findings clearly indicate that cortical contact area alone is insufficient to ensure superior primary stability when interference and canal morphology are unfavourable, and should not be interpreted as a general statement against increased cortical contact. Unwanted rotation during implantation, together with difficulties in achieving the planned final implant position, prevents precise alignment and reliable anatomical reconstruction - specifically femoral stem anteversion and leg length - which can directly influence patient pain and the risks of revision and re-revision due to instability and dislocation (Desai et al., 2013; Jo et al., 2015; Röder et al., 2012). The thin splines of the RAS design acted as guiding rails, minimizing angular distortion from the onset of implantation. Overclosure analysis showed a radial spline indentation of exactly 0.25 mm for the RAS design, matching the prominence of the thin splines and confirming the design rationale of the system. Overimpaction was prevented by the abrupt increase in contact from the wider splines once the reamed depth was reached.

During cyclic loading, both stem designs exhibited micromotion below 50 μm, which is the conservative limit for secondary osseointegration (Jasty et al., 1997; Kohli et al., 2021). At the higher load level, peaking at 200 % body weight, the solid design showed greater subsidence, consistent with the behavior during implantation. Two femurs implanted with the solid stem, which had shown minor to no relative motion at the lower load level (100 % body weight), fractured at the first loading sequence of the high load level. Both fractures were preceded by stem migration and increased relative motion rotationally (Fig. 9A). As a consequence of the loss of primary stability, the lever arm and such the bending moment increased from the anatomical 9° - 10° alignment, causing fractures of both femurs laterally (Fig. 9B).

The remaining solid stems showed significantly lower resistance to torsional loads during torque-to-failure testing. The thin splines of the RAS stem, designed for torsional resistance, combined with the increased press-fit of the second set of splines, resulted in nearly 10 Nm additional torque required to disrupt the bone–implant interface. However, with an average torque to failure of approximately 30 Nm for the remaining solid design, the increased cortical contact area of this design was able to withstand the physiological loads encountered during a standard gait cycle even without splines (Huber and Morlock, 2022). Instrumented-implant studies have reported torsional moments around the femoral stem of approximately 20–30 Nm for typical patient body weights, and up to roughly 40–60 Nm during demanding strengthening or aerobic exercises (Hafer et al., 2021). Against this background, the average torque to failure of approximately 30 Nm for the remaining solid design suggests that, even with reduced press-fit, this configuration can withstand the torsional demands of normal gait but may offer only a limited safety margin towards the upper range of physiologically plausible loads in heavier or more active patients, whereas the RAS design, with an approximately 10 Nm higher failure torque, provides a proportionally larger reserve capacity. Hip contact forces of up to about 900 % body weight have been observed during uncontrolled stumbling, indicating that such rare extreme events may still generate loads beyond the failure levels assessed here, so that the present torque-to-failure values should be interpreted as representative primarily of everyday and moderately demanding activities rather than catastrophic loading scenarios (Schwachmeyer et al., 2013). Consequently, the present data may underestimate the best-case stability of solid stems at higher press-fit levels, if those could be achieved safely. The comparison between the two designs such reflects the combined effect of spline geometry and press-fit magnitude, which limits direct conclusions to the effect of either factor.

The cavity and cortical contact analysis revealed non-homogeneous interaction between both designs and the reamed femoral canal, reflecting the uneven canal morphology at least up to the proximal diaphysis, where reaming for the standard stem length typically ends. Although the literature often advocates circumferential contact over 4 cm (Moriarty et al., 2020) or more, in practice – even with the improved accessibility of the femur and canal in in-vitro experiments as in this study compared to surgical reality – the natural non-uniformity of the femoral cavity does not permit such extensive bone removal without risking periprosthetic fractures due to cortical weakening. A slight deviation between the axis of the reamed cavity and that of the native

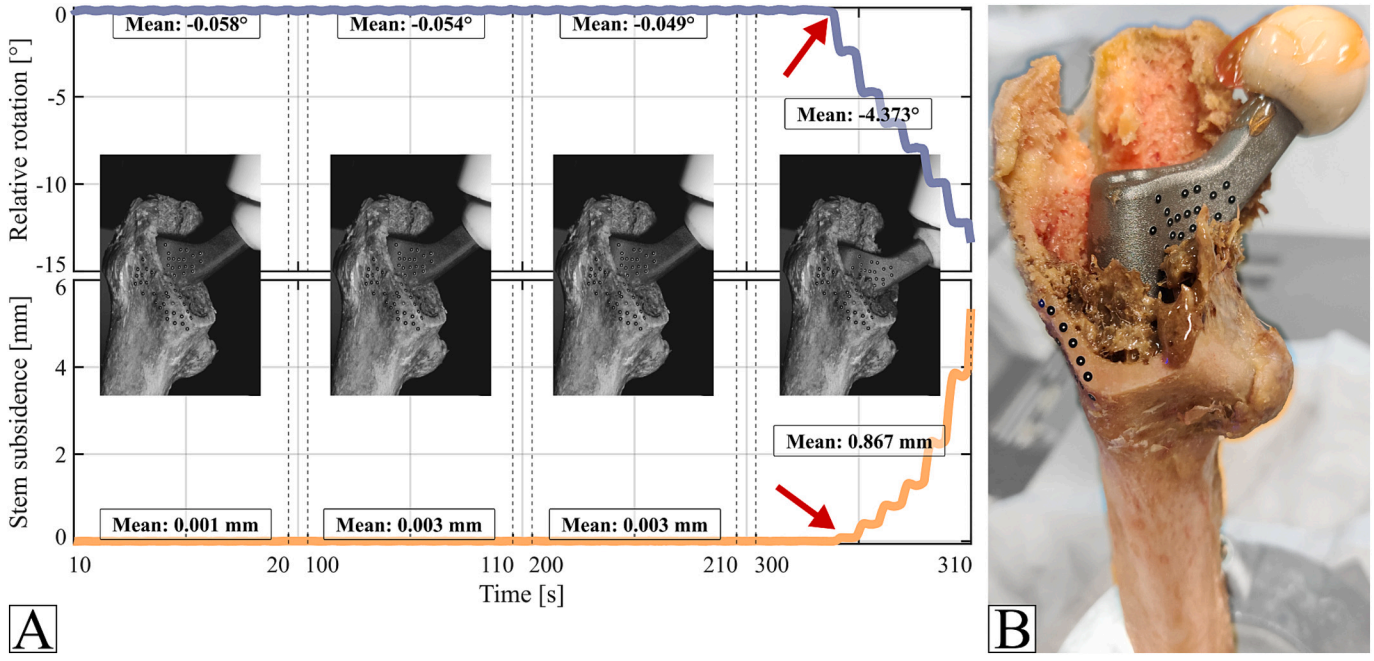

Fig. 9. Two of the ten femurs implanted with the solid stem fractured during cyclic loading compared to no fractures with the RAS design in a similar fashion. The results for one fracture are shown as an example. (**A**) The fracture was preceded by stem subsidence and rotation at the first interval of the second load level (indicated by red arrows, 1600 N peak force), whereas during the lower load level minimal instability occurred. (**B**) Both femurs fractured laterally after the instability increased the lever arm and such the bending moments under the altered load conditions.

canal was also observed. This deviation is likely more pronounced for longer straight stems due to the femur's natural curvature, resulting in a three-point scratch-fit, as reported in other studies (Frangie et al., 2022). The analysis of stem-cortex engagement in this study supports that canal non-roundness and axis deviation hinder the formation of a truly uniform circumferential wedge, so that "global" cortical contact is effectively reduced to a few discrete regions, which is consistent with the known clinical problem of three-point fixation in long revision stems. In this context, the solid stem design requires extensive, relatively uniform cortical contact to be stable; in theory, axial subsidence should cease once the tapered stem is fully wedged, but achieving this idealised seating position intraoperatively is difficult, as the overseating from the planned position in the study showed. By contrast, the RAS design is more forgiving, as the thin splines cut into the cortex and generate localised, circumferentially distributed indentations which compensate for canal irregularities and reduce the need for a long, continuous diaphyseal contact zone, while requiring less force to achieve the desired seating position in the femoral canal. The higher cumulative implantation force for the RAS compared to the solid design arises from the increased press-fit and the final impaction hits, when some wider, less-prominent splines already engage the cortex, abruptly increasing the contact area.

No significant influence of cortical BMD or bone morphology (Dorr classification) on cyclic-loading or torque-to-failure was observed, in contrast to a previous study comparing two revision hip stems with and without a second set of thin splines (Boettcher et al., 2023, 2025). This likely reflects the larger design differences evaluated in the present work, which outweighed the influence of bone quality and morphology. Despite the higher mean donor age, both cortical and trabecular BMD were relatively high, which can be attributed to the predominance of male donors (8/10) in the cohort. They also showed a low variability. No specimen had to be categorised as having low BMD and would thus have been clinically eligible for a cemented revision stem according to the Paprosky classification (Della Valle and Paprosky, 2003, 2004). The sex distribution and rather high bone quality limit the generalizability of our findings to elderly osteoporotic revision cases, for which a lower primary stability and higher susceptibility to intraoperative or early post-operative fractures must be anticipated, especially in patients with pronounced cortical thinning. In younger patients with higher BMD and thicker cortices, the primary stability of both stem designs would be expected to be likely superior, so that the present results should be be regarded as a conservative estimate for this group.

5. Conclusions

Maximising cortical contact through implant design in cementless hip arthroplasty with Wagner-like revision stems is not resulting in better primary stability since the native bone morphology precludes reliable circumferential bone–implant contact in the absence of splines. Only a combination of thin splines and increased cortical contact provides superior primary stability, as was demonstrated in comparison to conventional splined designs (Boettcher et al., 2023, 2025). Splines are particularly important for rotational locking and precise positioning during implantation (Amanatullah et al., 2015; Moriarty et al., 2020). A second set of less-prominent splines further facilitates to reach the desired seating position: as soon as they get in contact with the cortex, the sudden rise in insertion force provides a clear tactile endpoint, reliably preventing overimpaction.

CRediT authorship contribution statement

Julius M. Boettcher: Writing – review & editing, Writing – original draft, Validation, Software, Project administration, Methodology, Investigation, Funding acquisition, Formal analysis, Data curation. **Kay Sellenschloh:** Writing – review & editing, Investigation. **Ana Cruz Pardos:** Investigation. **Gerd Huber:** Writing – review & editing, Supervision. **Benjamin Ondruschka:** Resources. **Michael M. Morlock:** Writing – review & editing, Supervision, Project administration, Funding acquisition.

Funding

General institutional support was received by J&J MedTech as well as the provision with surgical components and instruments relevant for this study.

Declaration of competing interest

The authors have the following competing interests: ACP is a paid consultant for J&J MedTech and receives speaker fees from Exatech, Stryker, Zimmer and Smith and Nephew. GH is an associate member of the board of the German Society for Biomechanics. BO is a board member of the German Society for Forensic Medicine. MMM is a paid consultant for J&J MedTech and receives research support as Principal Investigator from J&J MedTech, and Beiersdorf. He receives speaker fees from Aesculap, J&J MedTech, Zimmer, Peter Brehm, Corin, and Mathys and is on the editorial board of Trauma und Berufskrankheit.

Acknowledgements

The authors thank J&J MedTech for providing prosthetic components, surgical instruments and institutional financial support. J&J MedTech was not involved in data evaluation or writing of the manuscript.

References

AAOS, 2024. American Joint Replacement Registry: Annual Report 2024. Surgical Data to 31 December 2023. https://www.aaos.org/registries/publications/ajrr-annual-report/.

Amanatullah, D.F., Howard, J.L., Siman, H., Trousdale, R.T., Mabry, T.M., Berry, D.J., 2015. Revision total hip arthroplasty in patients with extensive proximal femoral bone loss using a fluted tapered modular femoral component. Bone Joint J. 97-B (3), 312–317. https://doi.org/10.1302/0301-620X.97B3.34684.

Bätz, J., Messer-Hannemann, P., Lampe, F., Klein, A., Püschel, K., Morlock, M.M., Campbell, G.M., 2019. Effect of cavity preparation and bone mineral density on bone-interface densification and bone-implant contact during press-fit implantation of hip stems. J. Orthop. Res. 37 (7), 1580–1589. https://doi.org/10.1002/jor.24288.

Boettcher, J.M., Sellenschloh, K., Huber, G., Ondruschka, B., Morlock, M.M., 2023. The influence of hip revision stem spline design on the torsional stability in the presence of major proximal bone defects. PLoS One 18 (9), e0291599. https://doi.org/10.1371/journal.pone.0291599.

Boettcher, J.M., Sellenschloh, K., Huber, G., Ondruschka, B., Morlock, M.M., 2025. A modified Wagner stem design increases the primary stability in Cementless revision hip arthroplasty. Arthroplasty Today 32, 101622. https://doi.org/10.1016/j.artd.2025.101622.

Böhm, P., Bischel, O., 2004. The use of tapered stems for femoral revision surgery. Clin. Orthop. Relat. Res. 420, 148–159.

Della Valle, C.J., Paprosky, W.G., 2003. Classification and an algorithmic approach to the reconstruction of femoral deficiency in revision total hip arthroplasty. J. Bone Joint Surg. Am. 85-A (Suppl. 4), 1–6. https://doi.org/10.2106/00004623-200300004-00001.

Della Valle, C.J., Paprosky, W.G., 2004. The femur in revision total hip arthroplasty evaluation and classification. Clin. Orthop. Relat. Res. 420, 55–62. https://doi.org/10.1097/00003086-200403000-00009.

Desai, A.S., Dramis, A., Board, T.N., 2013. Leg length discrepancy after total hip arthroplasty: a review of literature. Curr. Rev. Musculoskelet. Med. 6 (4), 336–341. https://doi.org/10.1007/s12178-013-9180-0.

Engh, C.A., Bobyn, J.D., Glassman, A.H., 1987. Porous-coated hip replacement. The factors governing bone ingrowth, stress shielding, and clinical results. J. Bone Joint Surg. British 69 (1), 45–55. https://doi.org/10.1302/0301-620X.69B1.3818732.

Engh, C.A., Glassman, A.H., Griffin, W.L., Mayer, J.G., 1988. Results of cementless revision for failed cemented total hip arthroplasty. Clin. Orthop. Relat. Res. 235, 91–110.

Frangie, R., Wagstaff, P.D., Ismaily, S.K., Han, S., Rodriguez-Quintana, D., Noble, P.C., 2022. The length of Diaphyseal contact of tapered fluted stems is highly dependent on canal morphology. J. Arthroplast. 37 (7S), S697–S702. https://doi.org/10.1016/j.arth.2022.03.041.

Gkiatas, I., Malahias, M.-A., Xiang, W., Meyers, K.N., Torres, L.A., Tarity, T.D., Rodriguez, J.A., Bostrom, M.P., Wright, T.M., Sculco, P.K., 2021. How does contact length impact titanium tapered splined stem stability: a biomechanical matched pair cadaveric study. J. Arthroplast. 36 (9), 3333–3339. https://doi.org/10.1016/j.arth.2021.04.013.

Graeff, C., Timm, W., Nickelsen, T.N., Farrerons, J., Marín, F., Barker, C., Glüer, C.C., 2007. Monitoring teriparatide-associated changes in vertebral microstructure by high-resolution CT in vivo: results from the EUROFORS study. J. Bone Miner. Res. Off. J. Am. Soc. Bone Miner. Res. 22 (9), 1426–1433. https://doi.org/10.1359/jbmr.070603.

Grimberg, A., Lützner, J., Melsheimer, O., Morlock, M., Steinbrück, A., 2024. Endoprothesenregister Deutschland (EPRD): Jahresbericht 2024, Berlin, 106 pp. https://www.eprd.de/.

Hafer, H., Popovic, S., Martin, F., Hardt, S., Winkler, T., Damm, P., 2021. In vivo loading on the hip joint in patients with total hip replacement performing gymnastics and aerobics exercises. Sci. Rep. 11, 13395. https://doi.org/10.1038/s41598-021-92788-7.

Hartwig, C.H., Böhm, P., Czech, U., Reize, P., Küsswetter, W., 1996. The Wagner revision stem in alloarthroplasty of the hip. Arch. Orthop. Trauma Surg. 115 (1), 5–9. https://doi.org/10.1007/BF00453209.

Hernández-Mateo, J.M., Orozco-Martínez, J., Matas-Díaz, J.A., Vaquero, F.J., Sanz-Ruiz, P., 2024. Comparison of cylindrical and tapered stem designs for femoral revision hip arthroplasty. JCM 13 (6). https://doi.org/10.3390/jcm13061745.

Huber, G., Morlock, M.M., 2022. Which length should the neck segment of modular revision stems have? Clin. Biomech. (Bristol, Avon) 94, 105286. https://doi.org/10.1016/j.clinbiomech.2021.105286.

ISO/TC 150 Implants for Surgery, 2020. Chirurgische Implantate - Partieller und totaler Hüftgelenkersatz - Teil 4: Bestimmung der Dauerwechselfestigkeit und Leistungsanforderungen an Hüftendoprothesenschäfte. International Organization for Standardization, Geneva, Switzerland.

Jasty, M., Bragdon, C., Burke, D., O'Connor, D., Lowenstein, J., Harris, W.H., 1997. In vivo skeletal responses to porous-surfaced implants subjected to small induced motions. JBJS 79 (5), 707–714. https://doi.org/10.2106/00004623-199705000-00010.

Jo, S., Jimenez Almonte, J.H., Sierra, R.J., 2015. The cumulative risk of re-dislocation after revision THA performed for instability increases close to 35% at 15years. J. Arthroplast. 30 (7), 1177–1182. https://doi.org/10.1016/j.arth.2015.02.001.

Jones, C.M., Acuña, A.J., Jan, K., Forlenza, E.M., Della Valle, C.J., 2025. Trends and epidemiology in revision Total hip arthroplasty: a large database study. J. Arthroplast. https://doi.org/10.1016/j.arth.2025.01.011.

Kelmer, G., Stone, A.H., Turcotte, J., King, P.J., 2021. Reasons for revision: primary Total hip arthroplasty mechanisms of failure. J. Am. Acad. Orthop. Surg. 29 (2), 78–87. https://doi.org/10.5435/JAAOS-D-19-00860.

Kendrick, J.B., Noble, P.C., Tullos, H.S., 1995. Distal stem design and the torsional stability of cementless femoral stems. J. Arthroplast. 10 (4), 463–469. https://doi.org/10.1016/S0883-5403(05)80147-0.

Kohli, N., Stoddart, J.C., van Arkel, R.J., 2021. The limit of tolerable micromotion for implant osseointegration: a systematic review. Sci. Rep. 11 (1), 10797. https://doi.org/10.1038/s41598-021-90142-5.

Lawrence, J.M., Engh, C.A., Macalino, G.E., Lauro, G.R., 1994. Outcome of revision hip arthroplasty done without cement. JBJS 76 (7), 965–973. https://doi.org/10.2106/00004623-199407000-00002.

Maharaj, G.R., Jamison, R.D., 1993. Intraoperative impact: characterization and laboratory simulation on composite hip prostheses. In: Jamison, R.D., Gilbertson, L. N. (Eds.), Composite Materials for Implant Applications in the Human Body: Characterization and Testing. ASTM International100 Barr Harbor Drive, PO Box C700, West Conshohocken, PA 19428-2959, pp. 98–108.

Moriarty, P., Sheridan, G.A., Wong, L., Guerin, S., Gul, R., Harty, J.A., 2020. Bicortical contact predicts subsidence of modular tapered stems in revision Total hip arthroplasty. J. Arthroplast. 35 (8), 2195–2199. https://doi.org/10.1016/j.arth.2020.03.047.

NJR, 2024. National Joint Registry: 21th Annual Report 2024. Surgical data to 31 December 2023. https://reports.njrcentre.org.uk/.

Pierson, J.L., Small, S.R., Rodriguez, J.A., Kang, M.N., Glassman, A.H., 2015. The effect of taper angle and spline geometry on the initial stability of tapered, splined modular titanium stems. J. Arthroplast. 30 (7), 1254–1259. https://doi.org/10.1016/j.arth.2015.01.054.

Regis, D., Sandri, A., Bonetti, I., Braggion, M., Bartolozzi, P., 2011. Femoral revision with the Wagner tapered stem: a ten- to 15-year follow-up study. J. Bone Joint Surg. British 93 (10), 1320–1326. https://doi.org/10.1302/0301-620X.93B10.25927.

Röder, C., Vogel, R., Burri, L., Dietrich, D., Staub, L.P., 2012. Total hip arthroplasty: leg length inequality impairs functional outcomes and patient satisfaction. BMC Musculoskelet. Disord. 13, 95. https://doi.org/10.1186/1471-2474-13-95.

Schroeder, S., Jaeger, S., Schwer, J., Seitz, A.M., Hamann, I., Werner, M., Thorwaechter, C., Santos, I., Wendler, T., Nebel, D., Welke, B., 2022. Accuracy measurement of different marker based motion analysis systems for biomechanical applications: a round robin study. PLoS One 17 (7), e0271349. https://doi.org/10.1371/journal.pone.0271349.

Schwachmeyer, V., Damm, P., Bender, A., Dymke, J., Graichen, F., Bergmann, G., 2013. In vivo hip joint loading during post-operative physiotherapeutic exercises. PLoS One 8 (10), e77807. https://doi.org/10.1371/journal.pone.0077807.

Sheth, N.P., Nelson, C.L., Paprosky, W.G., 2013. Femoral bone loss in revision total hip arthroplasty: evaluation and management. J. Am. Acad. Orthop. Surg. 21 (10), 601–612. https://doi.org/10.5435/JAAOS-21-10-601.

Streit, M.R., Haeussler, D., Bruckner, T., Proctor, T., Innmann, M.M., Merle, C., Gotterbarm, T., Weiss, S., 2016. Early migration predicts aseptic loosening of Cementless femoral stems: a long-term study. Clin. Orthop. Relat. Res. 474 (7), 1697–1706. https://doi.org/10.1007/s11999-016-4857-5.

Wagner, H., 1987. Revisionsprothese für das Hüftgelenk bei schwerem Knochenverlust. Der Orthopade 16 (4), 295–300.

Wagner, H., 1989. Revisionsprothese für das Hüftgelenk. Der Orthopade 18 (5), 438–453.